

# Fourier Transformed Into a New Man

Jonah Shoemaker<sup>1</sup>

<sup>1</sup>*Arizona State University, Tempe, AZ, USA, email jcshoema@asu.edu*

October 26, 2018

## Introduction

In x-ray diffraction experiments, it is both difficult and costly to conduct successful trials. Protein samples are time-consuming and expensive to produce, and much of the sample is sprayed wastefully without experiencing a successful collision event with an x-ray pulse. Thus, while it is useful to invent new delivery systems that increase the frequency of successful collisions, it is also prudent to come up with new methods to increase the amount of data obtained from each collision as well. In the latter interest, for my time with the BioXFEL organization this summer, I worked on developing algorithms in Python to utilize results obtained from an experimental setup in which multiple diffraction patterns were obtained from a single diffraction event. This process, called diffractive stereo imaging, utilizes a carefully placed mirror behind the sample to obtain two diffraction patterns from the same object, one that travels through the object as normal, and a second that reflects off the mirror first to diffract through the object from a different angle before being collected by the camera as well. Both of these diffraction events can potentially be used to reconstruct two views of the same object, which could double the amount of information obtained from each successful collision. However, since the intensity pattern collected by the camera only tells us the magnitudes of the x-ray waves hitting each pixel, the primary obstacle for reconstructing these images is the retrieval of the unknown x-ray phases through iterative processes.

## Iterative Phase Retrieval

A pulse of coherent x-rays hitting an object experiences changes in photon momenta due to elastic collisions with the electrons in the object that cause them "spread" into a diffraction pattern. This diffraction pattern can be captured by a camera, or detector, in a laboratory. Diffraction patterns on a surface are equal to the squared modulus of the complex disturbance function at any point  $(x, y)$  on the surface of the detector:

$$I(x, y) = |U(x, y)|^2$$

The disturbance function is equal to the Fourier transform of a 2-dimensional projection,  $A(x, y)$ , of the electron density,  $\rho(\vec{r})$ , that depends on the direction of the beam and the orientation of the object, evaluated at the frequencies  $f_X = x/(\lambda z)$  and  $f_Y = y/(\lambda z)$ :

$$U(x, y) = \mathcal{F}(A(x, y))$$

where

$$A(x, y) = \int_{-\infty}^{\infty} \rho(\vec{r}) dz$$

The 2-D projection of the electron density is thus equal to the inverse transform of the disturbance function:

$$A(\vec{r}) = \mathcal{F}^{-1}(U(x, y))$$

Therefore, using coherent x-rays to find an object's electron density is merely a matter of using the intensity distribution of its diffraction pattern to find its disturbance pattern. However, a diffraction pattern only tells us the magnitudes of each complex value in the disturbance pattern function, and every complex number has both magnitude and phase, so in order to find  $U(x, y)$ , we need to find its unknown phases. Thus, we have to use another known characteristic of the object in order to obtain a second constraint set.<sup>1</sup> The second constraint we can apply is the size of the object, commonly called the support, since the object's size is usually known. Even though this constraint applies to the electron density of the object rather than its disturbance pattern function, as the first constraint does, since

<sup>1</sup>A constraint set is essentially a set of all possible solutions that satisfy a particular constraint. In the case of the diffraction pattern, the constraint set consists of all disturbance patterns that have the same magnitudes, but with any phases; this is equivalent to the set of all images that give the same intensity pattern. For the support, the constraint set is all possible electron densities that are confined to the support boundaries.

the electron density and the disturbance pattern are conjugated through the Fourier transform, a constraint on a function consequently constrains its Fourier transform. Thus, by alternating between the two constraints<sup>2</sup>, we can sometimes converge onto a solution for the phases. However, if a constraint set is concave<sup>3</sup>, then it is possible to reach a point of stagnation, where the algorithm begins to repeatedly alternate back and forth between the same points on either set. The process is called iterative phase retrieval, and there are several algorithms designed to accomplish it. The first and simplest of these algorithms is the Error Reduction (ER) algorithm.

## Error Reduction Algorithm

Given the intensity pattern, we can obtain the magnitudes of the complex disturbance pattern function, and constrain our solution to all possible with the same magnitudes. If we treat this constraint as a linear operator,  $\mathcal{P}_M$ , we can represent it in two different ways<sup>4</sup>:

$$\mathcal{P}_M \doteq \mathcal{F}^{-1} |U_0(x, y)| e^{i\phi} \mathcal{F}$$

$\phi$  is the angle of the current Fourier transform of  $A(x, y)$ ,  $U(x, y)$ , and is given by

$$\phi = \tan^{-1} \frac{\mathcal{I}(U(x, y))}{\mathcal{R}(U(x, y))}$$

$U_0(x, y)$  is the original disturbance pattern magnitudes from the intensities gathered by the detector.

To summarize, we take the Fourier transform of a current attempt at a solution  $A(x, y)$  in order to bring it to the disturbance or "momentum" space, constrain it by resetting  $U(x, y)$  to the magnitudes of the original disturbance pattern while preserving the angles of the current attempt  $U(x, y)$ , and take the inverse transform in order to bring it back into the object or "position" space.

The second way in which we can represent  $\mathcal{P}_M$  is with

$$\mathcal{P}_M \doteq \mathcal{F}^{-1} \frac{|U_0(x, y)|}{|U(x, y)|} \mathcal{F}$$

---

<sup>2</sup>When alternating between constraint sets like this, one can visualize two blobs connected to one another at exactly one point. Starting from a point in either blob, we draw a line to the nearest point on the other blob. From there, we draw a second line from this point to the nearest point on the first set, and so on, until we hopefully reach the point the two sets share.

<sup>3</sup>A concave set can be visualized as a blob with an indent in it. If, for example, the constraint set for the disturbance pattern magnitudes had any two points within it on either side of such an indent such that a straight line between them passed outside of the blob, then it would impossible to pass from one of these points to the nearest point on the support constraint blob, and from there to the second point in the first blob.

<sup>4</sup>As an arbitrary choice, we will always treat our inputs as the 2-D projection of the electron density,  $A(x, y)$ , rather than the disturbance pattern  $U(x, y)$ .

It is easily verified using vector calculus that these are equivalent.

If we know the support, or size of the object, we can constrain our current solution  $A(x, y)$  with the linear operator  $\mathcal{P}_S$ , represented by

$$\mathcal{P}_S \doteq s(\vec{x})$$

$s(\vec{x})$  is the support function, and in many algorithms is given as simply

$$s(\vec{x}) = \begin{cases} 1 & \vec{x} \in \mathcal{S} \\ 0 & \vec{x} \notin \mathcal{S} \end{cases}$$

where  $\mathcal{S}$  is the surface within which we know the 2-D projection of the object resides.

Given a guess, or set of random values, for the electron density projection  $A(x, y)$ , the ER algorithm attempts to converge towards a solution by repeatedly applying  $\mathcal{P}_S$  and  $\mathcal{P}_M$ :

$$A_{n+1}(x, y) = \mathcal{P}_M \mathcal{P}_S A_n(x, y)$$

However, if one of the sets is concave, as the set for  $\mathcal{P}_M$  is, then there is a good chance this algorithm will stagnate and fail to reach a solution. To overcome this stagnation, we can use the more complicated Hybrid Input-Output (HIO) or Difference Map (DM) algorithms.

## Difference Map Algorithm

The DM algorithm attempts to "jump" out of a stagnation in order to seek out the solution from a different path. The  $\mathcal{P}_M$  and  $\mathcal{P}_S$  constraint operators are the same, but in addition, there are related modifiers  $f_M$  and  $f_S$  such that

$$f_M \doteq (1 + \alpha_M) \mathcal{P}_M - \alpha_M$$

$$f_S \doteq (1 + \alpha_S) \mathcal{P}_S - \alpha_S$$

In order to find the next iterate,  $A_{n+1}(x, y)$ , apply the formula:

$$A_{n+1}(x, y) = A_n(x, y) + \beta (\mathcal{P}_S f_M - \mathcal{P}_M f_S) A_n(x, y)$$

These  $f$  operators enable the algorithm to "jump" out of a stagnation by allowing the solution to "wiggle" a little bit. Adjusting the  $\beta$  and  $\alpha$  parameters directly affects the wiggle room of the DM algorithm; with  $\alpha_M$  and  $\alpha_S$  set equal to 0,  $f_M$  and  $f_S$  become equivalent to  $P_M$  and  $P_S$ ,

and the algorithm adds the commutator of  $P_M$  and  $P_S$  onto the previous iterate. If  $\beta$  is equal to 0, the algorithm becomes an identity operation and makes no progress.  $\alpha_M$  and  $\alpha_S$  are typically set equal to  $\pm 1/\beta$  respectively, and  $\beta$  is set to some value between 0 and 1, typically 0.9.

Once a desired number of iterates or level of convergence is reached, a final application of the  $f_M$  operator followed by the  $\mathcal{P}_S$  operator is required to yield the reconstructed complex image function of the 2-D projection of the object. Taking the absolute value of this final output yields an image that can then be analyzed<sup>5</sup>

The algorithm will converge onto a solution when the difference,  $\Delta A(x, y) = (\mathcal{P}_S f_M - \mathcal{P}_M f_S) A_n(x, y)$ , approaches 0, so that each iteration of the algorithm no longer alters the solution. Thus, to compute errors, the norm of the difference is recorded with each iterate.

The DM algorithm is much more robust at seeking convergence than the ER or HIO algorithms, both requiring fewer iterates and stagnating less frequently. As seen in the results below, when the algorithm reaches a point of stagnation, the errors will typically plateau for some time before dropping suddenly as it jumps out of the stagnation and approaches the solution from a different direction.

## Diffractive Stereo Imaging

In an attempt to collect two diffraction patterns off of each individual x-ray diffraction trial, a mirror can be placed at a  $45^\circ$  angle to the projection axis<sup>6</sup> behind the object. This will cause the x-ray beam, idealized as incoming plane waves, to not only diffract through the object head on, but to also diffract through it from behind, as the beam will reflect off of the mirror before hitting the object as well. An experiment can be set up in which the two paths can be collected on a single detector, with the main undiffracted part of the beam nudged into a beam-stop. The x-ray beam will experience a path length difference between these two paths, causing the second diffraction to arrive at the detector out

of phase with the first. It is possible, however, to measure the path length difference in the setup, and to take this phase difference into account when attempting to re-construct these two projections of the object. This method is called diffractive stereo imaging, as it uses two different diffraction patterns to image the object<sup>7</sup>.

Due to the mixed nature of the intensity pattern collected, the various iterative phase algorithms require some modifications. In general, each image is reconstructed separately, with the notable exclusion of the  $\mathcal{P}_M$ , and consequently  $f_M$ , operations. Since these two operators entail constraining the magnitudes of the disturbance pattern, and the recorded magnitudes are a mixture of the two separate projections, the average of the two<sup>8</sup> current projection estimates must be used to provide the current phase estimates. This new  $\mathcal{P}_M$  is given by

$$\mathcal{P}_M \doteq \mathcal{I} + \mathcal{F}^{-1} \left( |U(x, y)| e^{i\phi} - \mathcal{I} \right) \mathcal{F} c_1$$

where  $\mathcal{I}$  is the identity operator, and  $c_1$  is the average of the two current projection estimates:

$$c_1 = \frac{1}{2} \left( \psi_0(x, y) + \psi_1(x, y) \right)$$

Since the second diffraction pattern is out of phase, its support constraint operator needs to be applied by first putting it into phase<sup>9</sup>, then applying the support, then bringing it back out of phase in order to continue applying the  $\mathcal{P}_M$  operator correctly. Since it can only be phase-shifted in Fourier space, and the support can only be applied in image space,  $\mathcal{P}_S$  becomes for the second object:

$$\mathcal{P}_S \doteq \mathcal{F}^{-1} e^{izk_z} \mathcal{F} s(\vec{x}) \mathcal{F}^{-1} e^{-izk_z} \mathcal{F}$$

Otherwise, retrieving phases for an intensity pattern from two diffraction events is the same as for a single diffraction event. One can simply apply these tailored operators in a typical ER or DM algorithm without any further modifications, performing each step on both image reconstructions in turn, and averaging them to apply  $\mathcal{P}_M$  when needed.

<sup>5</sup>Usually, since the process's ability to converge on the exact solution is fairly random, the phases of an intensity pattern of an unknown object will be solved for by applying this algorithm a substantial number of times and averaging the results.

<sup>6</sup>Typically chosen to be the z-axis.

<sup>7</sup>Although the process's name implies otherwise, the method used to reconstruct the projections does not only apply to taking two diffraction patterns off of the same object. Remove the mirror and place two objects within the beam's path, but not too close to one another on the  $(x, y)$  plane, and the diffraction patterns from each could be collected on a single detector and used to find the separate projections.

<sup>8</sup>Although this method can be applied to any number of separate projections with a shared intensity pattern, not just two.

<sup>9</sup>See The Fresnel Propagator for a description on how to apply this phase shift.

## Error Metrics

To measure the accuracy of a final solution obtained from an IPA described above, the phase transfer retrieval function is often used, as it does not rely on a comparison to a known correct solution. Instead, it compares the magnitude of the average phases at each point of the solution obtained, taking the or

$$\Gamma(\vec{q}) = |\langle e^{i\phi(\vec{q})} \rangle|$$

Since the phase angle for a complex function can also be expressed as the sum of the function's normalized real and imaginary parts<sup>10</sup>, this can also be expressed as the magnitude of the average value of the disturbance function's normalized values at each point  $(x, y)$ . Therefore, the phase retrieval transfer function can also be expressed as

$$\Gamma(\vec{q}) = \left| \left\langle \frac{U(x, y)}{|U(x, y)|} \right\rangle \right|$$

The more random the phase angles are, the more likely it becomes that for any given  $\phi(x, y)$  obtained, there is a corresponding  $-\phi(x, y)$  at another point in the solution. Thus, the closer to 0 that  $\Gamma(\vec{q})$  is, the more likely it is that the phase angles obtained are still random and therefore not true solutions. However, if the phase angles obtained are true, then the average value given by the exponential will be 1.

Another error metric that applies to all of the algorithms above is to apply the  $\mathcal{P}_S$  operator to a final solution obtained, since this will allow the solution's Fourier magnitudes to diverge away from the  $\mathcal{P}_M$  constraint, and then to compare the two with a chi-squared analysis:

$$\mathcal{E}(\vec{q}) = \sqrt{\frac{\sum(I_{\text{data}}(\vec{q}) - I(\vec{q}))^2}{\sum(I_{\text{data}}(\vec{q}))^2}}$$

For the DM algorithm, once the algorithm approaches a solution, the difference term will approach 0. Therefore, an error metric that can be applied is to take the norm of the difference. This norm will go to 0 as the algorithm approaches the solution:

$$\Delta(x, y) = \|\mathcal{P}_S f_M A(x, y) - \mathcal{P}_M f_S A(x, y)\|$$

## Blind Spots, Noise, and Other Undesirables

When an XFEL is used to diffract through an object, the majority of the x-ray beam passes

through the object without any significant alteration in trajectory due to the object's electron densities. This extremely high energy beam must be coaxed into a beam-stop<sup>11</sup> in order to avoid damaging any equipment – if a beam-stop were not used, the beam would burn the detector. As a result, intensity patterns obtained from XFELs have a blind spot in their middle. This can often be dealt with by allowing the intensity magnitudes in this blind spot region to float from each iteration of the algorithm to the next – instead of constraining all of the magnitudes with the  $\mathcal{P}_M$  operation, one only constrains the known magnitudes, and allows the central region's magnitudes to retain whatever random values they obtained from the  $\mathcal{P}_S$  operations. So long as the blind spot isn't too large, this will usually compensate for this loss of information. The new  $\mathcal{P}'_M$  operator for the blind spot phase retrieval can be represented as

$$\mathcal{P}'_M \doteq \begin{cases} \mathcal{P}_M & \vec{q} \in \mathcal{M} \\ \mathcal{I} & \vec{q} \notin \mathcal{M} \end{cases}$$

where  $\vec{q}$  is an element of the Fourier space such that  $U(\vec{k})$  is the disturbance at point  $(x, y)$ ,  $\mathcal{I}$  is the identity operator, and  $\mathcal{M}$  is the domain of the disturbance function.

Noise is always present in diffraction images, whether it is due to the camera used, the lighting in the room, or other less predictable sources. In the context of this project, there was also noise in the diffraction image from flaws in the mirror used to reflect the x-ray beam. When it comes to noise in the image, there are numerous approaches to mitigating its effect, but no definitive methods for completely removing it. One method is to take several dark images<sup>12</sup>, average them together, and subtract the result from the diffraction image. This approach is fairly adept at accounting for lighting and camera noise. For the mirror noise, it is possible to fit a polynomial function to the noise splotch using a least-squares-fit approach and subtract this function from the diffraction image. For the other less predictable sources, the Finger Cross method is the standard approach<sup>13</sup>.

## The Ewald Sphere

If we assume the collisions between incident x-ray waves and the electrons of an object being illuminated to be elastic, which is a good approximation, then we know that any incident

<sup>10</sup>See Euler's formula.

<sup>11</sup>A block of lead or something similar.

<sup>12</sup>Images taken with no x-ray beam on.

<sup>13</sup>Cross your fingers and hope for the best.

x-ray wave with wave vector  $\vec{k}_0$  will hit the electron and bounce off with new wave vector  $\vec{k}'$ . We can think of this as the x-ray wave being absorbed by the electron and re-emitted with no loss of energy in some new direction  $\hat{x}$ , which could point in any direction from the electron. Essentially, in other words, we can treat the electrons in the object as radiating spherical waves when illuminated.

Since there is no loss of energy, we can replace  $\vec{k}'$  with  $k\hat{x}$ . Thus, the change in the x-rays' trajectories will be given by  $\vec{q} = k\hat{x} - \vec{k}_0$ . Since  $\hat{x}$  can point in any direction and has magnitude equal to  $k_0$ , all possible vector differences trace out a sphere with radius  $k$ . This is called the Ewald sphere, and the points on its surface are all part of the 3-dimensional Fourier transform of the object. However, they only make up part of the overall transform, and so one illumination only provides some of the information on the object's 3-dimensional structure.

If one can change the direction of the incoming x-rays, or the orientation of the object, one can construct a conglomerate sphere enclosing all of the Ewald spheres that result from each illumination performed. At least two enable the construction of such a resultant sphere, which will have a radius equal to  $2k$  or  $4\pi/\lambda$ . This sphere denotes the set of all points in the 3-dimensional transform of the object that are obtainable from an illuminating wave of length  $\lambda$ . Thus, in order to accrue more information on a particular object, one must take diffraction patterns of it in more orientations, and overlay the resulting Ewald spheres together.

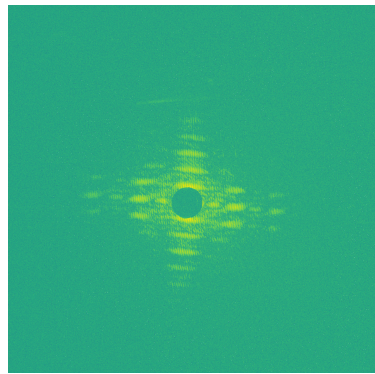
## Tilting the Detector

Due to the tilt of the CFEL plate and the mirror behind it at an angle of 45 degrees, some curvature was present in the fringes of the intensity pattern. Since this curvature was a result of the method used in collecting the intensity pattern, it is not present in the direct pattern that would be produced by the CFEL object and its reflection, and so is not accounted for by the phase retrieval algorithms described previously. Thus, this curvature needs to be corrected before the phases can be retrieved. Correcting this curvature entails taking all of the pixels on the two-dimensional camera plane as projections of an Ewald sphere, tilting this sphere by 45 degrees, and re-projecting it onto the two-dimensional surface. However, since the distance from the

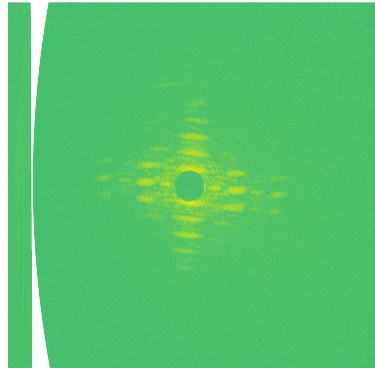
mirror to the camera is only known to a small degree of accuracy<sup>14</sup>, some method of testing for curvature, or lack thereof, needed to be used.

For this purpose, since the intensity pattern should be centro-symmetric, a test of centro-symmetry was used to select the most optimal Ewald sphere remapping. A series of distances were used within a range centered around the approximate measurement taken in the experiment to remap the intensity pattern, which was then inverted by 180 degrees and correlated with itself. The higher the correlation between the inverted remapping and the original, the more centro-symmetric the remapped image was, indicating that its Ewald curvature is more minimized. The best of these remapped outputs was selected for use in the phase-retrieval portion of the reconstruction.

Prior to remapping, the diffraction pattern's vertical fringes had visible curvature<sup>15</sup>:



After performing the centro-symmetry test on a range of camera distances, the best remapped result obtained had no noticeable curvature:



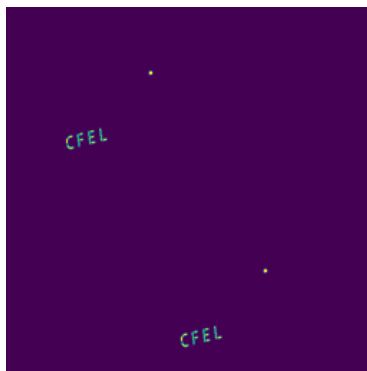
Since the micro-fringes running along each of the larger, horizontal "conglomerate" fringes are not themselves centro-symmetric, this is the most accurate result the sweep test is able to produce.

<sup>14</sup>It is important to note that this is not the same as the distance from the object to the mirror. See Simulating the Experimental Diffraction Pattern for further clarification.

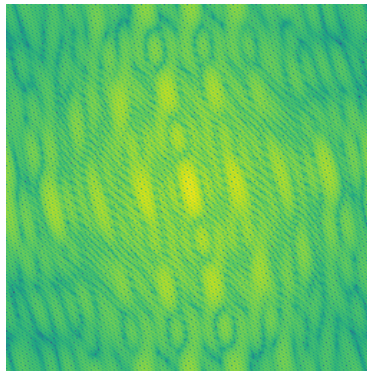
<sup>15</sup>The bright horizontal fringes that are above and below the beamstop

## Simulating the Experimental Diffraction Pattern

It is important to show, wherever possible, that the techniques and algorithms made to solve the experimental diffraction pattern work on a simulated diffraction pattern first. In order to simulate the diffraction pattern obtained experimentally, several imperfections described in section Blind Spots, Noise and Other Undesirables needed to be manually inserted into a simulated diffraction pattern. First, the CFEL logo and its blurred sister copy were inserted into a pad of zeros:



Then, the Fast Fourier Transform (FFT) function in the Numpy module was used to find the diffraction pattern for the combined pair of images, and its squared modulus was taken to get a simulated intensity pattern:



Next, since the experimentally obtained pattern had no useful information on its boundaries due to noise, a mask was applied to blank out the corners of the simulated pattern. In addition, the center of the pattern and a patch of noise due to another light source were also blanked:



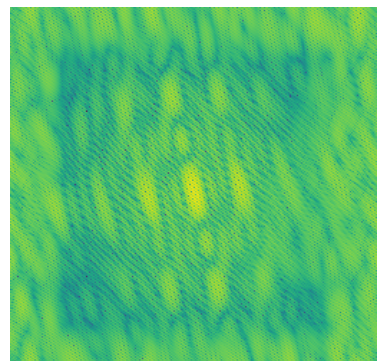
In addition, since the distance between the object and the mirror is used to re-focus the reflected image<sup>16</sup>, but isn't known to a high degree of accuracy in the experimental setup<sup>17</sup>, it was necessary to simulate an unknown mirror distance. To account for this unknown distance, a sweep similar to that mentioned in Tilting the Detector was utilized. Each mirror distance's Fresnel propagator term was used to perform a series of ER and DM iterations on the same randomly generated image solutions, and the propagator that produced the lowest RMS intensity error was used henceforth to attempt to reconstruct the images.

## Results

Using the Fresnel propagator obtained from the results of the sweep, after a few thousand iterations consisting of a mixture of ER and DM algorithm iterations, the following reconstruction was obtained:



This reconstruction re-produced the following intensity pattern:



<sup>16</sup>See Appendix, section 0.1.

<sup>17</sup>It is important to note that this distance is not the same as the distance from the mirror to the camera. See Tilting the Detector for further clarification.

With enough unmasked information and a good support, the algorithms are able to eventually fill in the incorrect masked intensity pixels with the correct values, as can be observed in the re-produced intensity pattern. With more iterations, this becomes more similar to the original unmasked intensity pattern.

## Future Direction

The next step is to take these simulation results and apply them to the real data. The Ewald sphere remapping gives an adequately

straightened intensity pattern to feed into the phase-retrieval process. The first step will be to smooth out the finer fringes within the broader fringes in the intensity pattern<sup>18</sup> and attempt to reproduce a single CFEL logo before attempting to solve for the reflection as well. Given that reconstruction of both images is possible, then the next step will be to take diffraction patterns of more complicated objects in the lab and attempt to reconstruct those. Comparing these reconstructions to one another could potentially give us more information on how beam damage acts on an object.

---

<sup>18</sup>These finer fringes are caused by the duplicate CFEL logos generated by both diffraction events, and so smoothing them out effectively serves to produce an intensity pattern from a single CFEL logo instead.

# Appendix

## 0.1 The Fresnel Propagator

Start with the plane wave function:

$$\psi(x, y, z) = \exp(i(k_X x + k_Y y + k_Z z))$$

It can easily be verified that this is a solution to the Helmholtz wave equation, so long as  $k_X^2 + k_Y^2 + k_Z^2 = k^2$ , where  $\vec{k}$  is the wave vector, equal to  $\frac{2\pi}{\lambda}$ . Solving for  $k_Z$  gives

$$k_Z = \sqrt{k^2 - k_X^2 - k_Y^2}$$

Put this into the plane wave equation to get

$$\psi(x, y, z) = \exp(i(k_X x + k_Y y)) \exp(iz\sqrt{k^2 - k_X^2 - k_Y^2})$$

Let there be an object, with the plane  $z = 0$  passing through it. Project the object onto the  $z = 0$  plane to get a 2-dimensional image of the object. Let the plane wave pass through the  $z = 0$  plane. The initial wavefront is then modeled by

$$\psi(x, y, 0) = \exp(i(k_X x + k_Y y))$$

If we want to examine this wavefront some distance further along the  $z$ -axis, at  $z = \Delta \geq 0$ , we just have to multiply the exponential containing  $k_Z$  back on:

$$\psi(x, y, 0) = \exp(i(k_X x + k_Y y)) \exp(iz\sqrt{k^2 - k_X^2 - k_Y^2})$$

This exponential term is the free space propagator.

If  $\tilde{\psi}(k_X, k_Y, 0) = \mathcal{F}\{\psi(x, y, 0)\}$ , then  $\psi(x, y, 0) = \mathcal{F}^{-1}\{\tilde{\psi}(k_X, k_Y, 0)\}$ . Therefore, we can write the initial wavefront in terms of its transform:

$$\psi(x, y, 0) = \frac{1}{2\pi} \int_{-\infty}^{\infty} \int_{-\infty}^{\infty} \tilde{\psi}(k_X, k_Y, 0) \exp(i(k_X x + k_Y y)) dk_X dk_Y$$

Each of the  $\exp(i(k_X x + k_Y y))$  terms is a boundary condition on the plane  $z = 0$  that leads to the 3-dimensional solutions  $\exp(i(k_X x + k_Y y + k_Z z))$ .

To obtain the wavefront some distance  $z = \Delta$  after the object's image, multiply by the free space propagator after having transformed  $\psi$  into Fourier space, but before inverse transforming it back:

$$\psi(x, y, 0) = \frac{1}{2\pi} \int_{-\infty}^{\infty} \int_{-\infty}^{\infty} \tilde{\psi}(k_X, k_Y, 0) \exp(i\Delta\sqrt{k^2 - k_X^2 - k_Y^2}) \exp(i(k_X x + k_Y y)) dk_X dk_Y$$

This allows us to define the free space propagation operator  $\mathcal{D}_\Delta$ :

$$\mathcal{D}_\Delta = \mathcal{F}^{-1} \exp(i\Delta\sqrt{k^2 - k_X^2 - k_Y^2}) \mathcal{F}$$

If the field is assumed to be paraxial, as it largely is in x-ray diffraction, then  $k_X$  and  $k_Y$  are much smaller than  $k_Z$ . This permits the use of a second-order Taylor series approximation:

$$\sqrt{1+x} = 1 + \frac{1}{2}x$$

Rearrange the expression for  $k_Z$  to get

$$k_Z = k \sqrt{1 + \frac{-k_X^2 - k_Y^2}{k^2}}$$

Apply the Taylor approximation:

$$k_Z \approx k \left( 1 + \frac{1}{2} \left( \frac{-k_X^2 - k_Y^2}{k^2} \right) \right)$$

$$k_Z \approx k - \frac{1}{2} \left( \frac{k_X^2 + k_Y^2}{k} \right)$$

Use this approximated expression to get the Fresnel propagation operator:

$$\mathcal{D}_\Delta^{(F)} = \mathcal{F}^{-1} \exp(ik\Delta) \exp \left( -i\Delta \frac{k_X^2 + k_Y^2}{2k} \right) \mathcal{F}$$

Since the first exponential term is a constant, and all of these transformations are linear, we can pull it out to the front:

$$\mathcal{D}_\Delta^{(F)} = \exp(ik\Delta) \mathcal{F}^{-1} \exp \left( -i\Delta \frac{k_X^2 + k_Y^2}{2k} \right) \mathcal{F}$$

The second exponential term,  $\exp \left( -i\Delta \frac{k_X^2 + k_Y^2}{2k} \right)$ , is the Fresnel propagator.

## 0.2 The Auto-Correlation Function and the FT of Intensity

The Fraunhofer diffraction equation tells us that, given an object illuminated in the  $(\xi, \eta)$  plane with disturbance pattern  $U(\xi, \eta)$ , the disturbance pattern on an observation plane  $(x, y)$  with normal distance  $z$  from the object plane will be given by the equation

$$U(x, y) = A(x, y) \int_{-\infty}^{\infty} U(\xi, \eta) e^{\frac{-i2\pi}{\lambda z}(x\xi + y\eta)} d\xi d\eta$$

where  $A(x, y)$  is a complex function of  $(x, y)$  alone.

It can be shown that this integral is equal to the Fourier transform of the disturbance pattern on the observation plane, evaluated at frequencies  $f_X = x/(\lambda z)$  and  $f_Y = y/(\lambda z)$ :

$$U(x, y) = A(x, y) \cdot \mathcal{F}\{U(\xi, \eta)\}$$

Let  $\mathcal{F}\{U(\xi, \eta)\} = G\left(\frac{x}{\lambda z}, \frac{y}{\lambda z}\right)$ . The observed intensity pattern at  $(x, y)$  is equal to the square modulus of the disturbance pattern, or

$$I(x, y) = \left| G\left(\frac{x}{\lambda z}, \frac{y}{\lambda z}\right) \right|^2$$

This can also be expressed as the product of  $G\left(\frac{x}{\lambda z}, \frac{y}{\lambda z}\right)$  with its complex conjugate,  $G^*\left(\frac{x}{\lambda z}, \frac{y}{\lambda z}\right)$ .

Henceforth, for simplicity, we will refer to  $G$  and  $G^*$  as functions of simply  $x$  and  $y$ .

Take the Fourier transform of the intensity pattern:

$$\mathcal{F}\{I(x, y)\} = \mathcal{F}\{G(x, y) \cdot G^*(x, y)\}$$

The modulation property of Fourier transforms states that the transform of a product of functions is equal to the convolution of each function's individual transform, or

$$\mathcal{F}\{G(x, y) \cdot G^*(x, y)\} = \mathcal{F}\{G(x, y)\} \circledast \mathcal{F}\{G^*(x, y)\}$$

Since  $G(x, y)$  is equal to  $\mathcal{F}\{U(\xi, \eta)\}$ , we use the duality property, which states that, if  $G(f_X, f_Y) = \mathcal{F}\{U(x, y)\}$ , then  $\mathcal{F}\{G(x, y)\} = U(-f_X, -f_Y)$ . Note the change of variables that takes place. Since the transform of a complex conjugate is equal to the complex conjugate of the transform, applying this property to our convolution above gives us

$$\mathcal{F}\{I(x, y)\} = U(-\xi, -\eta) \circledast U^*(-\xi, -\eta)$$

Since negating both variables  $\xi$  and  $\eta$  simply reflects the frame of reference of the object across the origin, the result above is equivalent to the disturbance pattern of the object convolved with itself, which is the auto-correlation function of the object. Therefore, the Fourier transform of a Fraunhofer diffraction pattern is equal to the auto-correlation of the object.

### 0.3 The Projection Slice Theorem

The Projection Slice Theorem states that taking a function of  $n+1$  dimensions, projecting it onto  $n$  dimensions, and taking the Fourier transform of the result is equivalent to taking an  $n+1$  dimensional Fourier transform of the function and then slicing it through its origin parallel to the original projection.

Take a 3-dimensional function  $f(x, y, z)$ . Project it onto 2 dimensions by integrating it across  $z$ :

$$\int_{-\infty}^{\infty} f(x, y, z) dz = f'(x, y)$$

Now take the Fourier transform of the result:

$$\mathcal{F}\{f'(x, y)\} = \int_{-\infty}^{\infty} \int_{-\infty}^{\infty} f'(x, y) \exp(-2\pi i(xf_X + yf_Y)) dx dy$$

or

$$\mathcal{F}\{f'(x, y)\} = \int_{-\infty}^{\infty} \int_{-\infty}^{\infty} \left\{ \int_{-\infty}^{\infty} f(x, y, z) dz \right\} \exp(-2\pi i(xf_X + yf_Y)) dx dy$$

Now, take the 3-dimensional Fourier transform of the original function:

$$\mathcal{F}\{f(x, y, z)\} = \int_{-\infty}^{\infty} \int_{-\infty}^{\infty} \int_{-\infty}^{\infty} f(x, y, z) \exp(-2\pi i(xf_X + yf_Y + zf_Z)) dx dy dz$$

Slice this on the  $(f_X, f_Y)$  plane through the origin by setting  $f_Z = 0$ :

$$\mathcal{F}\{f(x, y, z)\} = \int_{-\infty}^{\infty} \int_{-\infty}^{\infty} \int_{-\infty}^{\infty} f(x, y, z) \exp(-2\pi i(xf_X + yf_Y)) dx dy dz$$

Rearrange the limits of integration to integrate  $f(x, y, z)$  across  $dz$  first in order to get the same result as above.

Therefore, taking a 2-dimensional projection, such as a 3-dimensional object seen from only one side, and Fourier transforming the result gives the intensity pattern of a diffraction through the object, which is equal to a 2-dimensional slice through the Fourier transform of the 3-dimensional object distribution.

## Acknowledgements

I would like to thank the NSF organization for allowing me to do this internship. In addition, I would like to thank my PI, Rick Kirian, and the BioXFEL post-doctorate Joe Chen, who played a significant role in mentoring me over this internship as well. Lastly, I would like to thank Nadia Zatsepina and Ganesh Subramanian for their contributions.

Coherent X-Ray Optics by David Paganin was used to research the subject matter reported in this presentation.